



## Finite element analysis of thermal buckling in automotive clutch plates

Jiaxin Zhao, Zhuo Chen, Huizhou Yang & Yun-Bo Yi

To cite this article: Jiaxin Zhao, Zhuo Chen, Huizhou Yang & Yun-Bo Yi (2016) Finite element analysis of thermal buckling in automotive clutch plates, Journal of Thermal Stresses, 39:1, 77-89, DOI: [10.1080/01495739.2015.1123590](https://doi.org/10.1080/01495739.2015.1123590)

To link to this article: <https://doi.org/10.1080/01495739.2015.1123590>



Published online: 28 Jan 2016.



Submit your article to this journal [↗](#)



Article views: 195



View related articles [↗](#)



View Crossmark data [↗](#)



Citing articles: 10 View citing articles [↗](#)

# Finite element analysis of thermal buckling in automotive clutch plates

Jiaxin Zhao, Zhuo Chen, Huizhou Yang, and Yun-Bo Yi

Department of Mechanical and Materials Engineering, University of Denver, Denver, Colorado, USA

## ABSTRACT

A finite element analysis is performed to investigate the stability boundaries of thermal buckling in automotive clutches. It is found that the radial variation of temperature considerably affects the critical buckling temperature. A linear or monotonic temperature profile always leads to a dominant coning mode. Whereas a temperature profile with the maximum temperature located in the middle leads to a dominant non-axisymmetric buckling mode, and the associated critical temperature is typically much higher. The numerical solutions for periodic variations of temperature with multiple waves along the circumference were also tentatively obtained.

## ARTICLE HISTORY

Received 26 January 2015  
Accepted 5 April 2015



## KEYWORDS

Eigenvalue method; finite element analysis; thermal buckling; thermal stresses

## Introduction

It is well known that automotive brakes and clutches can fail at elevated temperatures and thermal stresses due to the frictional heat generation at the contact surfaces during brake operations or clutch engagements. The mechanism of failure, however, varies depending on the operating conditions. The most important failure mechanisms include thermoelastic instability or hot spotting [1, 2], thermal cracks [3] and thermal buckling [4]. Among them, thermal buckling is believed to be one of the dominant failure mechanisms in clutch plates due to their small thicknesses. Briefly a sufficiently large temperature gradient in the radial direction can result in the circumferential or “hoop” thermal stress that leads to the loss of structural stability in some extreme cases [5]. The buckling phenomenon in clutches often occurs in two different modes, namely the *coning* mode and the *potato chip* mode [6]. Higher-order buckling modes can also occur in the presence of either the radial or circumferential thermal stresses. The primary objective of research on thermal buckling is to find the critical temperature gradient above which the system loses stability, along with the associated deformed shape.

Despite its significant importance in automotive applications, thermal buckling has not been thoroughly investigated especially for clutches, which is somewhat surprising. Pioneering research was conducted by Audebert et al. [6], who presented both analytical and numerical methods to predict thermal buckling of a clutch disk due to thermoelastic/plastic residual stresses. The Timoshenko beam theory [7] was applied on a curved beam assuming that the beam may buckle laterally at a certain critical value of the bending moment. However, the variation in the thermal stress along the radial direction was not considered in the theory. Ma [8] extended the method to automotive disk brakes and investigated the effect of geometric and material parameters on the critical buckling loads via the finite element method [9]. These studies revealed that both axisymmetric and non-axisymmetric buckling modes can be caused by a uniformly distributed thermal loading in the circumferential direction. In addition, a slightly changed temperature profile in the radius can greatly affect the deformed shape of the buckling mode.

**CONTACT** Jiaxin Zhao  [jiaxin1773@gmail.com](mailto:jiaxin1773@gmail.com)  Department of Mechanical and Materials Engineering, University of Denver, Denver, Colorado 80208, USA.

Color versions of one or more of the figures in the article can be found online at [www.tandfonline.com/uths](http://www.tandfonline.com/uths).

In the present work, we incorporate the methodologies used in Ma's work and target investigating thermal buckling in clutches in a more systematic way by taking into account the effects of various temperature profiles. We are particularly interested in the effect of those profiles resembling thermoelastic instability induced "banding modes" and "hot spots" [10], and we believe that the two phenomena can be coupled together at certain temperature ranges. It is noticed that a clutch plate can usually be approximated as an annular ring. Therefore it would be beneficial to take advantage of the symmetry in the geometry. When the thermal loading and the deformed shape are both uniformly distributed in the circumference, the axisymmetric elements can be used to discretize the geometry on the cross-sectional plane only, and can therefore simplify the model and reduce the computational effort. However, a traditional axisymmetric model is inappropriate for the cases where the deformation and the stress distribution are non-axisymmetric. Hence, in a more general case, a full three-dimensional finite element model will be implemented to investigate those buckling modes at higher orders.

### Finite element approach

Buckling is caused by the geometric nonlinearity in a deformed structure, which is equivalent to adding an additional stiffness term to the system. The general finite element formulation of the buckling problems thus involves the construction of *stress stiffness matrix*  $[k_\sigma]$  that is added to the stiffness matrix  $[k]$ . This stress stiffness matrix is then used to develop an eigenvalue equation for the buckling load [11]. More specifically, the structure is first loaded with a reference load to find the reference stress stiffness matrix,  $[K_\sigma]_{ref}$ . Another load  $\{R\} = \lambda\{R\}_{ref}$  will then be applied to the structure, where  $\lambda$  represents an arbitrary multiplier to the original reference load. Correspondingly the stress stiffness matrix is related to the applied load and becomes  $[K_\sigma] = \lambda[K_\sigma]_{ref}$ . Therefore the following two equations can be established.

$$([K] + \lambda_{cr}[K_\sigma]_{ref}) \{D\}_{ref} = \lambda_{cr}\{R\}_{ref} \quad (1)$$

$$([K] + \lambda_{cr}[K_\sigma]_{ref}) \{\{D\}_{ref} + \delta D\} = \lambda_{cr}\{R\}_{ref} \quad (2)$$

where  $\{\delta D\}$  is the buckling displacement. The subtraction of them leads to

$$([K] + \lambda_{cr}[K_\sigma]_{ref}) \{\delta D\} = \{0\} \quad (3)$$

This equation defines an eigenvalue problem, in which the term  $\lambda_{cr}$  is the eigenvalue and  $\{R\}_{cr} = \lambda_{cr}\{R\}_{ref}$  is the buckling load, which can be caused by any type of mechanical load, including thermal stresses. The above formulation has been fully integrated into the commercial code ABAQUS [12]. The leading eigenvalues and the corresponding eigenvectors are determined iteratively from a generalized eigenvalue equation. These eigenvalues are the load multipliers and the eigenvectors are expressed in terms of the nodal displacement components.

As a clutch disk has an annular shape with dimensions in both thickness and diameter, a three-dimensional (3-D) geometry is the first and natural choice to develop a numerical model. However, a clutch plate has a thin thickness compared to the other dimensions, and the stress/strain distributions across the thickness are usually negligible. We can therefore focus our attention on the temperature gradient in the radial and circumferential directions only. Due to this reason we may also use a reduced two-dimensional (2-D) shell model. Furthermore, if the thermal load and the buckling shape are both axisymmetric, using an axisymmetric element type can considerably improve the numerical accuracy and efficiency. We will therefore develop three different finite element models, namely 3-D, 2-D and axisymmetric models, to investigate and compare the effects of dimensionality on the numerical solutions. Schematics of these models are shown in Figures 1 and 2. A clutch plate can be partially constrained especially at the inner radius in some situations. These constraints may raise the buckling load significantly. For simplicity we assume free boundary conditions here for all cases, and therefore the results obtained actually represent lower bounds to the solutions.

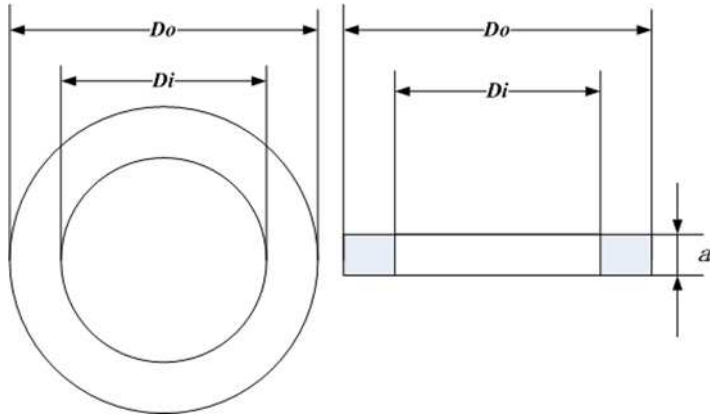


Figure 1. Schematic of a clutch plate.

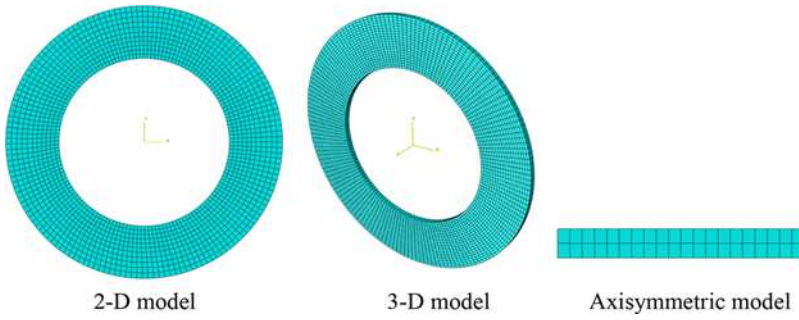


Figure 2. Finite element models for thermal buckling analysis.

In ABAQUS there are various types of elements available in the element library. To compare the convergence performance in the solution we use some representative types and numbers of elements. It is well known that linear interpolating shape functions can cause *shear locking* in the solution [13]; therefore, we select the quadratic element C3D20R in the 3-D model, representing 20-node quadratic brick elements with reduced integration. For the 2-D model, we use the general shell element S4R (4-node general-purpose shell, reduced integration with hourglass control, finite membrane strains). For the axisymmetric model, we use the quadratic element type CAX8R (i.e., 8-node bi-quadratic, reduced integration). Examples of element types are illustrated in Figure 2.

### Analytical approximation

For the purpose of comparison and validation, an analytical approach has been developed on the basis of Timoshenko's beam theory. The fundamental assumption here is to approximate the annular ring geometry as a curved beam. According to Audebert et al. [6], the critical moments can be expressed as

$$M_c^* = \frac{1+K}{2} \pm \sqrt{\left(\frac{1-K}{2}\right)^2 + KN^2} \quad (4)$$

$$K = \frac{1+\nu}{2} \quad (5)$$

$$M_c = \frac{2M_c^* G(R_o - R_i)a^3}{3(R_o + R_i)} \quad (6)$$

where  $M_c^*$ ,  $M_c$ ,  $K$ ,  $N$ ,  $\nu$  are the dimensionless critical buckling moments, the critical buckling moments, the stiffness ratio, the buckling wave number and Poisson's ratio, respectively.  $G$ ,  $a$ ,  $R_o$ ,  $R_i$  represent the shear modulus, the cross-section thickness, the outer radius and the inner radius of the annular disk, respectively. According to the critical moment equation Eq. (4), when the wave number  $N = 1$ , the critical moment  $M_c^* = 0$ , which indicates that it is a rigid body mode that has no effect on the elastic stability. Consequently, we can predict that the first two dominant buckling modes are the "coning" mode ( $N = 0$ ) and the "potato chip" mode ( $N = 2$ ). When  $N = 0$ , the critical moment equation becomes,

$$M_c^* = K \quad (7)$$

when  $N = 2$ , the critical moment is,

$$M_c^* = \frac{1 + K}{2} - \sqrt{\left(\frac{1 - K}{2}\right)^2 + 4K} \quad (8)$$

The thermal stress distribution in the beam can be solved from the temperature distribution, which is then used to find the bending moment by integration. The in-plane moment caused by the circumferential stress can be expressed as [7],

$$M = \int_{R_i}^{R_o} a\sigma(r) \left(r - \frac{R_o + R_i}{2}\right) dr \quad (9)$$

where  $\sigma(r)$  represents the thermal stress along the circumferential direction. When the free boundary conditions are applied at the inner and outer radii,  $\sigma(r)$  can be expressed as,

$$\sigma(r) = \frac{\alpha E}{r^2} \int_{R_i}^r r T dr - \alpha E T + \frac{EC_1}{1 - \mu} + \frac{EC_2}{(1 + \mu)r^2} \quad (10)$$

$$C_1 = \frac{\alpha}{2(1 - \mu)} \frac{1}{R_o^2 - R_i^2} \int_{R_i}^{R_o} T r dr \quad (11)$$

$$C_2 = \frac{\alpha(1 + \mu)R_i^2}{R_o^2 - R_i^2} \int_{R_i}^{R_o} T r dr \quad (12)$$

If we assume a linear temperature gradient in radius,

$$T = \Delta T \frac{r - R_i}{R_o - R_i} \quad (13)$$

where  $\Delta T$  represents the temperature gradient. Based on the above equations, the critical temperature gradient can be determined.

## Computational results

### Convergence studies

A set of convergence studies have been performed via the finite element analysis. Here we use the same material and geometric parameters as in Ma's research [8] for the purpose of comparisons. These parameters are shown in Table 1. A linear reference temperature gradient is assumed along the radius direction as follows:

$$T = 50 \frac{r - 0.08}{0.13 - 0.08} \quad (14)$$

According to Table 1, the inner radius is 0.08 m and the outer radius is 0.13 m. Therefore the temperature varies from zero at the inner radius to 50 at the outer radius. No constraints are placed at either inner or outer radius.

**Table 1.** Geometric and material parameters of the computational model used in the convergence study.

Inner diameter Di (mm)	Outer diameter DO (mm)	Thickness a (mm)	Young's modulus E (GPa)	Poisson's ratio $\nu$	Thermal expansion coefficient $\alpha (K^{-1})$
160	260	6	110	0.3	$1.25 \times 10^{-5}$

Three different element types, S4R, CAX8R, C3D20R have been investigated and compared. Meanwhile different numbers of elements have been used in the three dimensions, along the thickness, the radius and the circumference, respectively. The different combinations of element types and element numbers used are explained in Table 2. The eigenvalues obtained from the thermal buckling analysis are presented in Figure 3.

According to Figure 3, we can have the following conclusions: (1) Axisymmetric element type CAX8R gives an accurate result for mode 1 (coning mode) with even a very coarse mesh ( $2 \times 4$ ); (2) With a medium-size mesh ( $1 \times 10 \times 48$ ), 3-D element C3D20R leads to a converged result consistent with that of CAX8R; (3) Shell element S4R provides a relatively small error of approximately 0.33% with a fine mesh ( $14 \times 96$ ); (4) The element number in the thickness direction has little effect on the result. It should be pointed out that although the axisymmetric element type is the most efficient one, it can only be used for the study of coning modes in which the mode shape is also axisymmetric at the same time.

To validate our finite element model, here we compared the critical buckling temperatures computed from the finite element analysis with analytical solutions. The comparison is shown in Table 3. According to the table, the largest discrepancy between the finite element result using the S4R elements and the analytical solution is merely 2.7%, which can be considered acceptable. This comparison has shown that the shell element S4R is appropriate for the current study.

Based on the above conclusions, we will use the shell element S4R with a relatively fine mesh ( $14 \times 96$ ) throughout the following discussions.

**Table 2.** Different element types and numbers used in the convergence study.

Element type	1	2	3	4	5	6
S4R	$4 \times 16$	$6 \times 24$	$8 \times 32$	$10 \times 48$	$12 \times 64$	$14 \times 96$
C3D20R	$1 \times 4 \times 16$	$1 \times 6 \times 24$	$1 \times 8 \times 32$	$1 \times 10 \times 48$	$1 \times 12 \times 64$	$1 \times 14 \times 96$
C3D20R (4 Elements along thickness)	$4 \times 4 \times 16$	$4 \times 6 \times 24$	$4 \times 8 \times 32$	$4 \times 10 \times 48$	$4 \times 12 \times 64$	$4 \times 14 \times 96$
CAX8R	$2 \times 4$	$2 \times 6$	$2 \times 8$	$2 \times 10$	$2 \times 12$	$2 \times 14$

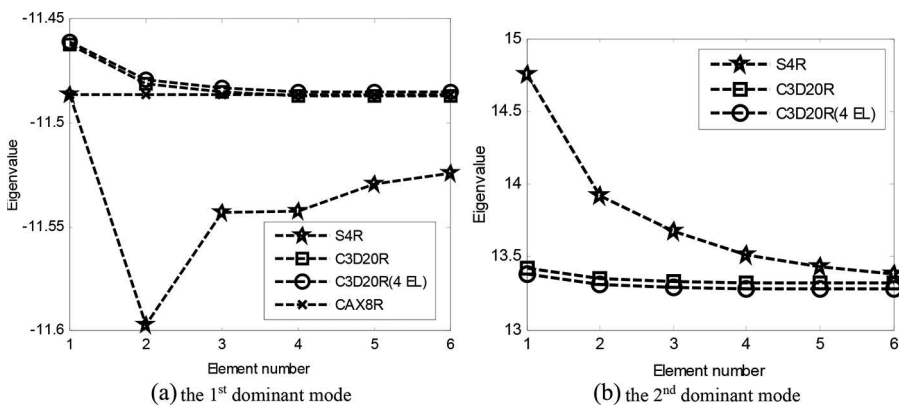


**Figure 3.** Convergence studies of the finite element models.

**Table 3.** A comparison of the critical buckling temperature computed by the finite element method and the analytical method.

Mode	Analytical solution	Ma's solution	FE (S4R)
1	-557.1	-575	-576.2
2	683.0	687.5	668.8

### Effects of different patterns of temperature distribution

Automotive transmission clutches undergo different operating conditions, such as the initial engagement, full contact and plate separation stages. As a result, various temperature distributions in the clutch plates are possible. Linear, exponential and sinusoidal distributions have been found among the most representative temperature profiles. The linear distribution can be caused by the sliding speed as a linear function of the radius and by the fact that the frictional heat generation rate is a linear function of the sliding speed. The sinusoidal distribution is related to the local high-temperature regions known as hot spots that could be excited by thermoelastic instability. An exponential distribution can be caused by the non-uniform convective cooling on the plate surface or a non-uniform contact pressure during the engagement and separation of plates. Additionally, the temperature gradient may exist in both radial and circumferential directions. It is possible that the temperature patterns have some effects on the thermal buckling mode and the buckling temperatures, so we choose various temperature patterns and compute the eigenvalues of thermal buckling. To obtain a more accurate result, we use the parameters [1] from a realistic clutch that are shown in Table 4.

### Monotonic radial temperature variations

Here we assume a temperature distribution monotonically changing from the inner to the outer radius. We investigate three different scenarios:

$$T_1 = 39 \frac{r - 0.086}{0.125 - 0.086} \quad (15)$$

$$T_2 = 39 \sin(40.2768(r - 0.086)) \quad (16)$$

$$T_3 = \frac{39(\exp(60(r - 0.086)) - 1)}{240.5436(0.125 - 0.086)} \quad (17)$$

where  $T_1$ ,  $T_2$ ,  $T_3$  represent, respectively, linear, sinusoidal and exponential temperature distributions that are also illustrated in Figure 4. We chose the constants in these functions in such a way that all three functions have the same temperature difference of 39°C across the radius.

The eigenvalues and the buckling temperatures computed by ABAQUS are shown in Table 5 and Figure 5. It is noticed that some of the eigenvalues and temperature gradients are negative, representing that the temperature decreases from the inner to outer radius. According to Table 5, the buckling temperature is typically very low for a monotonic temperature profile. The lowest buckling temperature is around 178°C, which is well below the maximum operating temperature of a clutch plate.

According to Figure 5, the temperature distribution pattern has a limited effect on the buckling temperature. As the buckling temperatures of Mode 1 and Mode 2 are the lowest, these two modes are the leading modes. This is consistent with the conclusions obtained in previous researches. The first

**Table 4.** Geometric and material parameters of a realistic clutch plate used in the parametric studies.

Inner diameter $d_i$ (mm)	Outer diameter $d_o$ (mm)	Thickness $a$ (mm)	Young's modulus $E$ (GPa)	Poisson's ratio $\nu$	Thermal expansion coefficient $\alpha$ ( $K^{-1}$ )
172	250	3	160	0.29	$1.27 \times 10^{-5}$

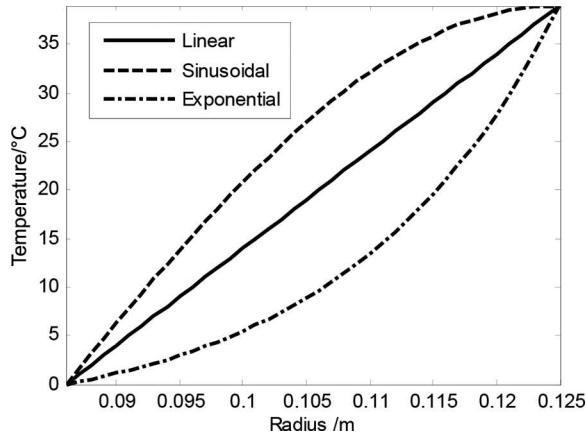


Figure 4. Monotonic temperature profiles along radius.

Table 5. Buckling eigenvalues of the monotonic radial temperature profiles.

Mode	Eigenvalue		
	Linear	Sinusoidal	Exponential
1	-4.556	-4.838	-4.916
2	5.444	5.332	5.741
3	10.92	10.82	11.32
4	-11.73	-11.09	-12.99
5	16.49	16.54	16.81

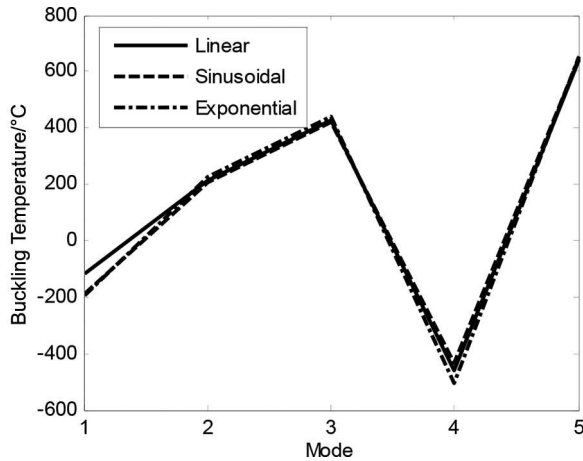


Figure 5. Buckling temperatures of the monotonic radial temperature profiles.

two buckling modes of thermal distribution are shown in Figure 6. In this figure, the first two thermal buckling modes are always the axisymmetric mode (coning mode) and the non-axisymmetric mode (potato chip mode) in the condition that the temperature increases or decreases with the radius monotonically. Meanwhile, the coning mode can appear only if the temperature at the inner radius is the highest. In addition, it is obvious that the deformed shape changes with different thermal patterns. Therefore, we can conclude that the different thermal patterns that increase or decrease monotonically along the radius direction have significant effects on the deformed shape rather than the thermal buckling temperature.



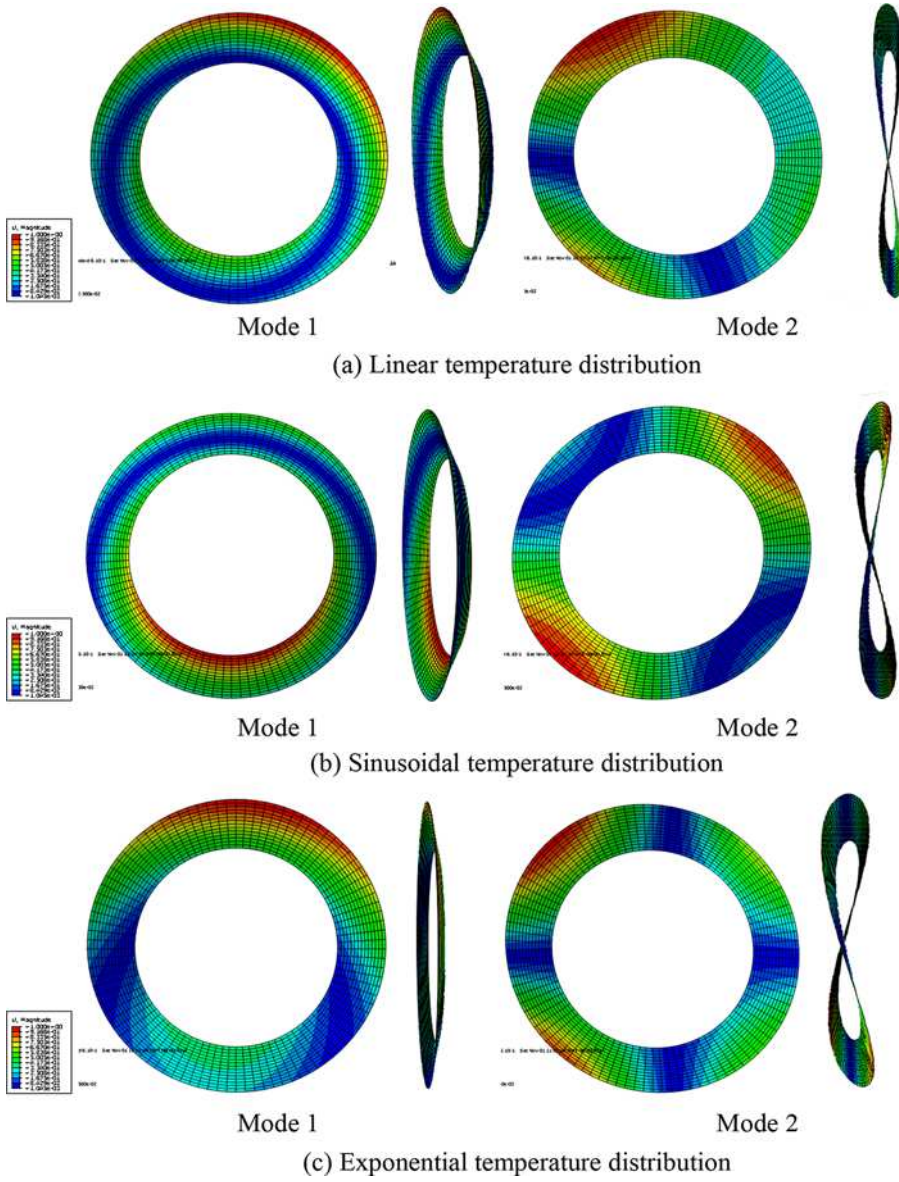


Figure 6. Buckling modes of the monotonic radial temperature profiles.

**Non-monotonic radial temperature variations**

To explore the phenomenon further, we assumed a different thermal profile pattern along the radius, in which the highest temperature is located at the mean radius, instead of the inner or outer radius. We made three different assumptions on the temperature distributions as expressed in the following functions

$$T_4 = \begin{cases} \frac{78(r - 0.086)}{0.125 - 0.086}, & (0.086 \leq r \leq 0.1055) \\ 78 - \frac{78(r - 0.086)}{0.125 - 0.086}, & (0.1055 \leq r \leq 0.125) \end{cases} \tag{18}$$

$$T_5 = 39 \sin(80.5536(r - 0.086)) \tag{19}$$

$$T_6 = \begin{cases} \frac{39(\exp(120(r - 0.086)) - 1)}{240.544(0.125 - 0.008)}, & (0.086 \leq r \leq 0.1055) \\ \frac{39(\exp(120(-r + 0.125)) - 1)}{240.544(0.125 - 0.008)}, & (0.1055 \leq r \leq 0.125) \end{cases} \quad (20)$$

where  $T_4, T_5, T_6$  are, respectively, linear, sinusoidal and exponential temperature distributions that are shown in Figure 7. We chose the constants in these functions in such a way that all three functions have the same temperature difference of 39°C between the inner and the mean radii, which is consistent with the previous case of monotonic distribution. We follow the same procedure to perform the finite element analysis. The obtained eigenvalues and buckling temperatures are shown in Table 6 and Figure 8.

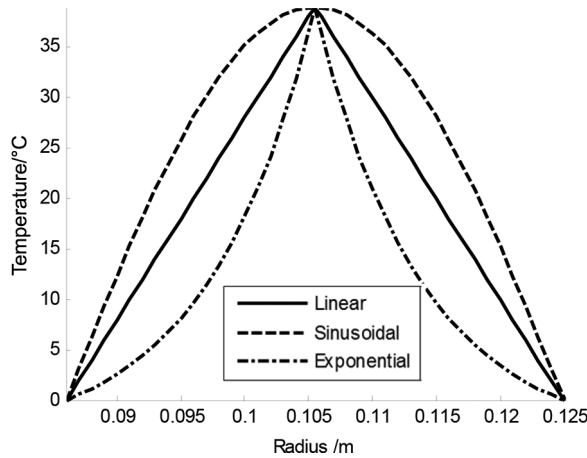


Figure 7. Non-monotonic radial temperature profiles.

Table 6. Buckling eigenvalues of the non-monotonic radial temperature profiles.

Mode	Eigenvalue		
	Linear	Sinusoidal	Exponential
1	-46.21	-42.51	-53.25
2	-56.14	-51.69	-64.59
3	-61.88	-56.94	-71.23
4	-67.05	-61.63	-77.29
5	69.62	64.56	79.17

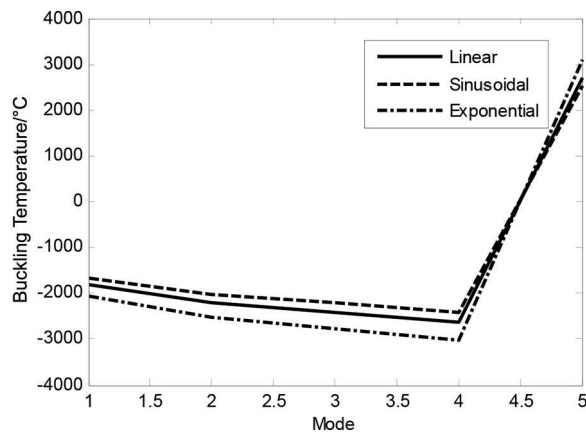


Figure 8. Buckling temperatures of the non-monotonic radial temperature profiles.

According to Figure 8, when the highest temperature is located at the mean radius, the effect of thermal patterns on the critical buckling temperature is not significant. Compared to Tables 5 and 6, it is clear that the eigenvalues of this case are much larger than those under monotonic temperature distributions. For example, when the temperature distribution is a piecewise linear function, the eigenvalue of Mode 1 here is approximately 10 times greater than that of monotonic temperature profile. In fact, the typical value of the buckling temperature for non-monotonic temperature profiles is well above the operating temperatures of automotive clutches. Hence thermal buckling is more probable to take place under monotonic radial temperature profiles as opposed to non-monotonic temperature distributions.

We also investigate the deformed shapes of the first two dominant modes that have the lowest buckling eigenvalues, as shown in Figure 9. In the figure it is clear that Mode 1 of all three thermal patterns has a

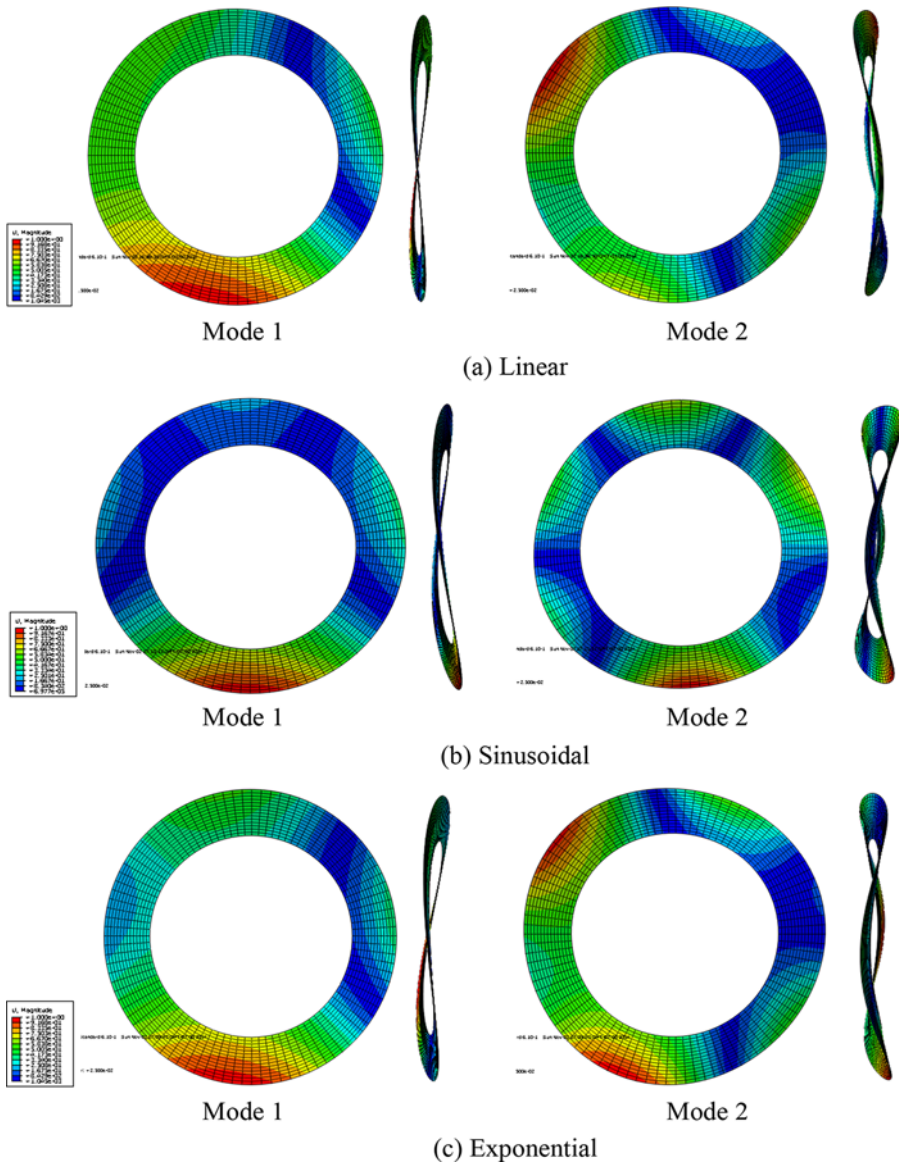


Figure 9. Buckling modes of the non-monotonic radial temperature profiles.

“potato chip” shape and Mode 2 is a higher order one with more waves in the circumference. Meanwhile, the buckling shape varies with different thermal patterns. Consequently, we can conclude that the shape of the thermal pattern mainly affects the deformed shape rather than the buckling temperature. Finally, the axisymmetric coning mode cannot take place in a condition that the highest temperature is located in the middle of the radius.

**Circumferential temperature variations**

The temperature gradient may also exist in the circumferential direction. Here we first assume a sinusoidal and linear thermal distributions that have the same maximum temperature difference in the following form:

$$T_7 = 39 \sin(n\theta) \quad n = 0.5, 1.5 \tag{21}$$

where  $\theta$  and  $n$  represent, respectively, the angular position and the wave number. The buckling eigenvalues computed from the finite element analysis are reported in Table 7. According to the table, roughly speaking there is a trend in the buckling temperature to increase with the wave number. For example, the buckling temperature of mode 1 is 1785°C at  $n = 1.5$ , and 1071°C at  $n = 0.5$ . In general the buckling temperature here is much higher than those of the monotonic radial profile. However, some values are still below 1000°C and this can come close to the vicinity of the maximum operating temperature in some extreme cases.

The eigenvectors of the first two modes are shown in Figure 10. For an integer wave number greater than one, inconsistent solutions were obtained using different finite element mesh sizes. Some of them were apparently erroneous. This was possibly caused by the numerical convergence issues in the eigenvalue solver employed by ABAQUS. We suspect that under a periodic temperature distribution along the circumference, the material expands in the hot region and contracts in the cold region. These thermal effects will counteract each other and eventually cancel out, leading to an unconditional stable situation. But the results are not conclusive in this work due to the insufficient evidence available. In contrast, a temperature distribution of non-integer wave number can lead to buckling, although this scenario is very rare in practical applications.

In addition to sinusoidal variations, we investigated a different periodic temperature distribution with the following piecewise linear function in the circumferential direction,

$$T_8 = \begin{cases} \frac{39\theta}{\pi}, & (0 \leq \theta \leq \pi) \\ 78 - \frac{39\theta}{\pi}, & (\pi \leq \theta \leq 2\pi) \end{cases} \tag{22}$$

The corresponding buckling eigenvalues are reported in Table 7. Obviously, the buckling temperatures are much higher than those of the sinusoidal counterpart. The lowest buckling temperature is above 1000°C, which is higher than the typical operating temperature of clutch systems. Again, we also encountered the numerical convergence problems in this case. We will investigate this issue in more detail in the future.

**Table 7.** Buckling eigenvalues of the sinusoidal and linear temperature profiles in the circumference ( $n$  is the wave number).

Mode	Eigenvalue		$T_8$
	$n = 0.5$	$n = 1.5$	
1	27.46	45.76	57.60
2	43.43	71.52	90.61
3	60.36	98.70	126.26
4	63.03	105.1	132.65

The first two columns are the sinusoidal profile; the last column is the linear profile with  $T_8$  defined in Eq. (22).

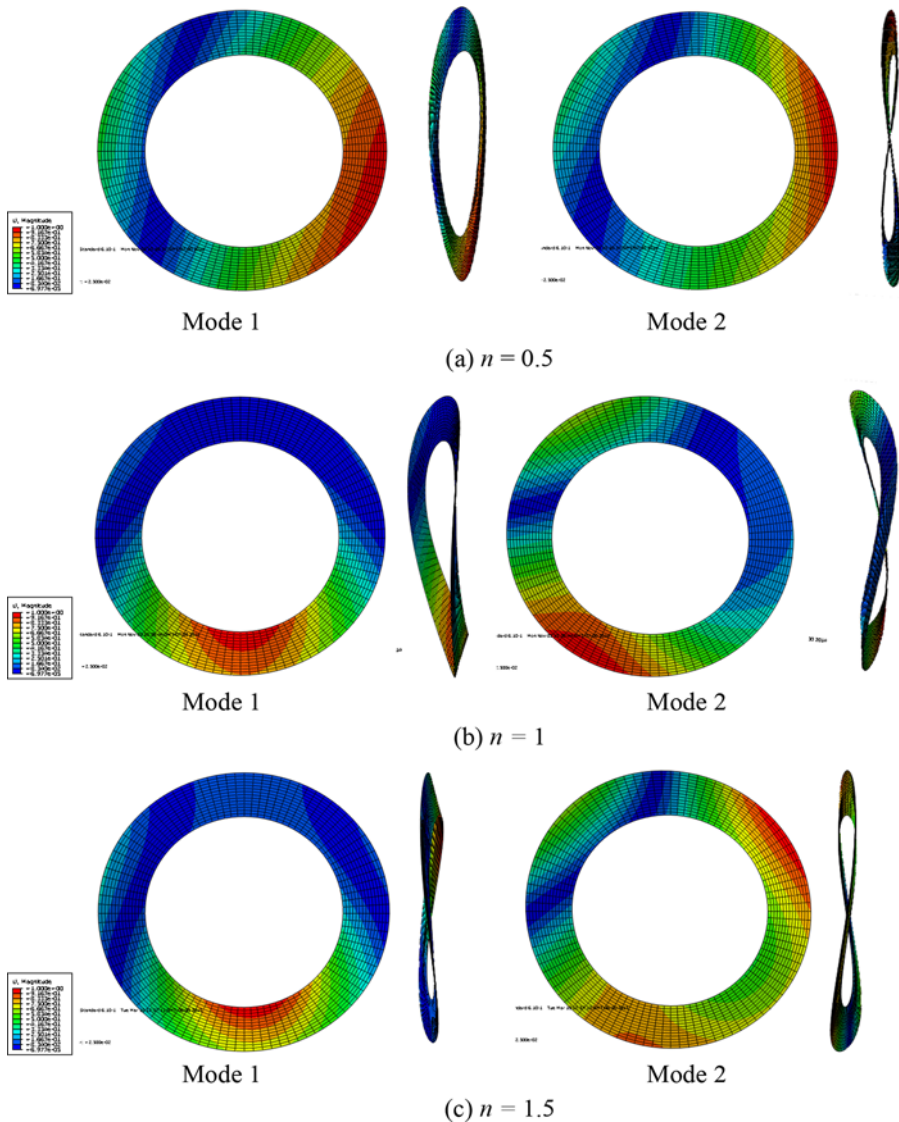


**Figure 10.** Dominant buckling modes of the sinusoidal temperature distributions along the circumference.

## Conclusions

We have investigated the thermal buckling phenomenon of disk clutches via a finite element analysis. It has been found that buckling can occur when the temperature distribution is uniform in the circumference but non-uniform in the radius. The critical buckling load and the dominant buckling mode shapes are significantly affected by the patterns of radial temperature distribution. For a linear profile of temperature, the axisymmetric coning mode has the lowest buckling temperature and the corresponding highest temperature always occurs at the inner radius. The non-axisymmetric potato chip modes also exist, but occur at higher buckling temperatures. For nonlinearly distributed temperature where the maximum temperature is located neither at the inner or outer radius, the non-axisymmetric buckling mode will be dominant and the corresponding buckling temperature is typically much higher than that of linearly distributed temperature profile.

We also found that slightly changed temperature distribution with the same temperature difference (e.g., linear, sinusoidal and exponential distributions with the same magnitude and location of the maximum temperature) can greatly impact the thermal buckling mode shapes but they have very close eigenvalues, implying that their effects on the buckling temperatures are limited. On the other hand, a periodic temperature variation with multiple hot spots in the circumference may never lead to buckling, even though the result is still inconclusive due to some numerical difficulties in the computation.

It should be pointed out that thermoelastic instability can be induced at the beginning of frictional sliding, and can result in both banding modes and focal hot spots. In comparison, thermal buckling takes place only when the temperature gradient exceeds a critical value, and therefore it can hardly occur at the beginning of clutch engagement.

## References

1. J. Zhao, B. Ma, and H. Li, Investigation of Thermoelastic Instabilities of Wet Clutches, in *Assembly and Manufacturing (ISAM) 2013 IEEE International Symposium*, pp. 69–72, 2013.
2. J. Zhao, B. Ma, H. Li, and Y. Yi, The Effect of Lubrication Film Thickness on Thermoelastic Instability under Fluid Lubricating Condition, *Wear*, vol. 303, pp. 146–153, 2013.
3. A. E. Anderson and R. A. Knapp, Hot Spotting in Automotive Friction Systems, *Wear*, vol. 135, pp. 319–337, 1990.
4. T. K. Kao, J. W. Richmond, and A. Douarre, Brake Disc Hot Spotting and Thermal Judder: An Experimental and Finite Element Study, *Int. J. Vehicle Design*, vol. 23, pp. 276–296, 2000.
5. P. Zagrodzki, Numerical Analysis of Temperature Fields and Thermal Stresses in the Friction Discs of a Multidisc Wet Clutch, *Wear*, vol. 101, pp. 255–271, 1985.
6. N. Audebert, J. R. Barber, and P. Zagrodzki, Buckling of Automatic Transmission Clutch Plates due to Thermoelastic/Plastic Residual Stresses, *J. Thermal Stresses*, vol. 21, pp. 309–326, 1998.
7. S. P. Timoshenko and J. M. Gere, *Theory of Elastic Stability*, Courier Dover Publications, Mineola, New York, 2009.
8. C. Ma, *Thermal Buckling of Automotive Brake Discs*, Ph. D. Thesis, University of Michigan, Ann Arbor, Michigan, 2004.
9. L. C. Wellford and G. M. Dib, Finite Element Methods for Nonlinear Eigenvalue Problems and The Postbuckling Behavior of Elastic Plates, *Comput. Struct.*, vol. 6, pp. 413–418, 1976.
10. Y. B. Yi, J. R. Barber, and P. Zagrodzki, Eigenvalue Solution of Thermoelastic Instability Problems Using Fourier Reduction, *Proc. Roy. Soc. Lond. A*, vol. 456, pp. 2799–2821, 2003.
11. R. D. Cook, *Concepts and Applications of Finite Element Analysis*, John Wiley & Sons, Hoboken, New Jersey, 2007.
12. Simulia DS. Abaqus User's Manual (ed. 6.9), Providence, RI. [www.simulia.com](http://www.simulia.com). Accessed May, 2011.
13. Y. B. Yi and M. A. Matin, Eigenvalue Solution of Thermoelastic Damping in Beam Resonators using a Finite Element Analysis, *J. Vibr. Acoust.*, vol. 129, pp. 478–483, 2007.